Characterization and Finite Element Modeling of Galfenol Minor Flux Density Loops

Zhangxian Deng, Marcelo J. Dapino

Smart Vehicle Concepts Center, Department of Mechanical and Aerospace Engineering
The Ohio State University, Columbus, OH, USA, 43210

ABSTRACT

This paper focuses on the development of a three-dimensional (3D) hysteretic Galfenol model which is implemented using the finite element method (FEM) in COMSOL Multiphysics. The model describes Galfenol responses and those of passive components including flux return path, coils and surrounding air. A key contribution of this work is that it lifts the limitations of symmetric geometry utilized in the previous literature and demonstrates the implementation of the approach for more complex systems than before. Unlike anhysteretic FEM models, the proposed model can simulate minor loops which are essential for both Galfenol sensor and actuator design. A group of stress-flux density loops for different bias currents is used to verify the accuracy of the model in the quasi-static regime.

Keywords: Galfenol, Finite Element Method, COMSOL Multiphysics, Hysteresis

1. INTRODUCTION

Magnetostrictive gallium-iron alloys, known as Galfenol, are a recent class of smart materials that are promising for sensing and actuation applications. To optimize the design of Galfenol sensors and actuators, system level models combining constitutive Galfenol modeling and passive system components are essential. Further, such models must be able to describe both minor and major magnetization excursions as this is the way Galfenol systems are often operated in practice.

Evans and Dapino[1]proposed a high accuracy, computationally efficient model which uses energy averaging (EA) considering local energies near Galfenol's six easy crystallographic directions. Evans[2] derived a two dimensional (2D) static hysteretic finite element model for axisymmetric geometries. This model has been proved by Liang and Dapino[3] for unimorph beam vibrations under a constant field assumption. Chakrabarti and Dapino[4] simplified the EA model for axisymmetric 2D geometries such as those encountered in hydraulically-amplified Terfenol-D actuators. Although the model incorporates magnetic hysteresis, its application to general 3D geometries requires some additions. Chakrabarti and Dapino[5] later formulated a 3D model for both static and dynamic operation, and implemented it in COMSOL Multiphysics. However, the model was formulated for anhysteretic responses in order to reduce computational complexity. It is emphasized that the response of Galfenol force sensors usually is in the form of minor loops, the nuances of which anhysteretic models cannot accurately describe.

To overcome these limitations, a 3-D hysteretic FEM model is presented in this paper. Fig. 1 shows both the geometry in COMSOL and the device developed for experimental validation of the model.[6] The derivation process of weak forms, the modifications of the EA hysteretic Galfenol model, a model inversion procedure, and methods of improving convergence are presented in this paper. Quasi-static simulation results are compared with constant drive current measurements of stress-flux density minor loops on $< 100 >$ oriented textured polycrystalline $Fe_{18.4}Ga_{81.6}$.

Further author information: (Send correspondence to M.J.D)
Z.D.: E-mail: deng.92@osu.edu, Telephone: 1-614-886-1340
M.J.D.: E-mail: dapino.1@osu.edu, Telephone: 1-614-688-3689

Behavior and Mechanics of Multifunctional Materials and Composites 2013, edited by Nakhiah C. Goulbourne, Hani E. Naguib, Proc. of SPIE Vol. 8689, 86890V
© 2013 SPIE · CCC code: 0277-786X/13/$18 · doi: 10.1117/12.2012511

Downloaded From: http://proceedings.spiedigitallibrary.org/ on 07/12/2017 Terms of Use: http://spiedigitallibrary.org/ss/termsofuse.aspx

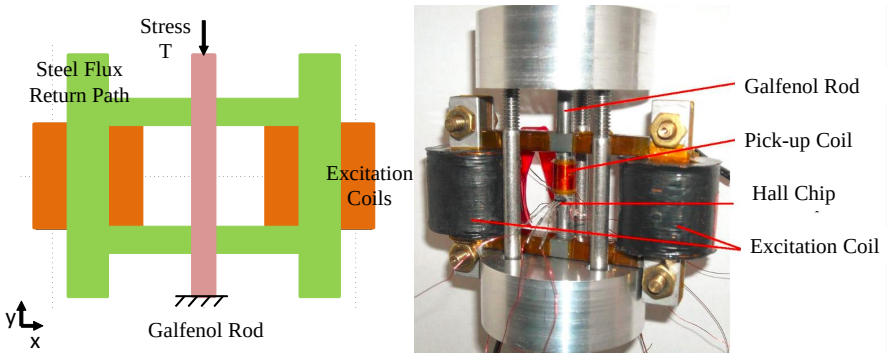

Figure 1. System geometry in COMSOL (left); Experiment set-up (right).

2. THEORY

2.1 Weak form equations

The response of the Galfenol testing system in Fig. 1 can be described using two physics, magnetic domain and structural mechanics domain. The magnetic domain is formulated on the basis of Maxwell's equations. To simplify the problem, displacement currents, Lorentz forces, and voltage gradients are neglected. With these assumptions, the weak form of magnetic physics can be written as[7]

$$\int_{V_B} \mathbf{H} \cdot \delta\mathbf{B} dV + \int_{V_B} \sigma \frac{\partial \mathbf{A}}{\partial t} \cdot \delta\mathbf{A} dV = \int_{\partial V_B} (\mathbf{H} \times \mathbf{n}) \cdot \delta\mathbf{A} d\partial V + \int_{V_B} \mathbf{J}_s \cdot \delta\mathbf{A} dV. \tag{1}$$

The weak form equation for structural mechanics is derived from Newton's law as

$$\int_{V_u} \mathbf{T} \cdot \delta\mathbf{S} dV + \int_{V_u} (\rho \frac{\partial^2 \mathbf{u}}{\partial t^2} + c\frac{\partial \mathbf{u}}{\partial t}) \cdot \delta\mathbf{u} dV = \int_{\partial V_u} \mathbf{t} \cdot \delta\mathbf{u} d\partial V + \int_{V_u} \mathbf{f}_B \cdot \delta\mathbf{u} dV. \tag{2}$$

The independent variables are the vector magnetic potential ($\mathbf{A}$) and the mechanical displacement field ($\mathbf{u}$).

2.2 Hysteretic EA model

(a) Hysteretic Model for Galfenol

A complete derivation of anhysteretic Galfenol model has been shown by Chakrabarti and Dapino.[5] Armstrong[8] first proposed a constitutive model for Terfenol-D using energy weighting. Evans[2] added stress-induced volume fraction change into the previous model, and successfully described the minor loops caused by stress variation. The volume fraction for hysteretic Galfenol responses is defined in an incremental form which includes both irreversible (hysteretic) and reversible (anhysteretic) volume fraction changes,

$$d\xi^k = (1-c)d\xi^k_{irr} + cd\xi^k_{an}, \tag{3}$$

where, $d\xi^k$ is the volume fraction increment along the k^{th} moment orientation. Here, $d\xi^k_{an}$ is the reversible volume fraction increment which can be written in analytical form. However, $d\xi^k_{irr}$, the irreversible volume fraction is calculated numerically as shown by Evans and Dapino.[9] The irreversible volume fraction maintains accuracy only when $d\mathbf{H}$ and $d\mathbf{T}$ are small enough,

$$\begin{aligned} d\xi^k_{irr} =& \frac{\zeta}{k_p}(\xi^k_{an} - \xi^k_{irr})[\mu_0 M_s(|dH_1| + |dH_2| + |dH_3|) + \\ & (3/2)\lambda_{100}(|dT_1| + |dT_2| + |dT_3|) + 3\lambda_{111}(|dT_4| + |dT_5| + |dT_6|), \end{aligned} \tag{4}$$

where ζ depends on the sign of susceptibility, k_p quantifies pining site density in the material, and c describes the fraction of reversible moment rotations.

Downloaded From: http://proceedings.spiedigitallibrary.org/ on 07/12/2017 Terms of Use: http://spiedigitallibrary.org/ss/termsofuse.aspx

(b) Material Jacobian Evaluation

Based on the anhysteretic Jacobian presented by Chakrabarti and Dapino,[5] a hysteretic Jacobian can be obtained through replacing the volume fraction term ξ_{an} by ξ,

$$\frac{d\xi^k}{dH_i} = (1-c)\frac{d\xi^k_{irr}}{dH_i} + c\frac{d\xi^k_{an}}{dH_i}, \quad i = 1,2,3, \tag{5}$$

$$\frac{d\xi^k}{dT_i} = (1-c)\frac{d\xi^k_{irr}}{dT_i} + c\frac{d\xi^k_{an}}{dT_i}, \quad i = 1,2,3,4,5,6. \tag{6}$$

Eq.(5) and Eq.(6) show that the derivatives are also defined in incremental form.

(c) Model Inversion

Fig. 2 illustrates the process of numerically approximating the weak form PDEs in COMSOL. It is noted that, unlike in the EA model, the independent variables are $(\mathbf{B}, \mathbf{S})$ and the dependent variables are $(\mathbf{H}, \mathbf{T})$. Hence, inversion of the EA model is necessary. It is not possible to derive analytical expressions for the inverse model from the EA model. A direct Newton method requiring calculation of the Jacobian matrix at each iteration step is not computationally efficient. Chakrabarti and Dapino[5]applied the SR1 quasi-Newton method in the 3D anhysteretic model using nonlinear material functions. This method has proven to be both efficient and accurate, but lack of convergence is observed when the field or stress is large enough to drive the material to saturation.

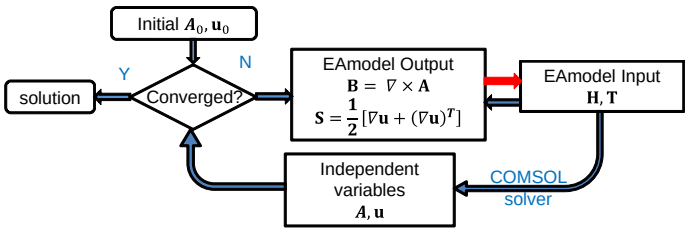

Figure 2. Flowchart of COMSOL simulation.

Fig. 3 shows the flowchart of the SR1 quasi-Newton method applied in this study. To address the convergence issues, the following modifications are necessary. First, the initial conditions are set to be the model results in the previous step instead of all zeros. Second, values of $(\mathbf{H}, \mathbf{T})$ and $(\mathbf{B}, \mathbf{S})$ should be rescaled so that inputs and outputs of the inverse model are of the same order. After applying Eq.(7), where SX and SY are the scaling matrix for inputs and outputs respectively, model convergence is achieved. Third, a varying α is used such that it always satisfies the Wolfe condition. At last, Trust-Region-Reflective (TRR) method is required for special points where the quasi-Newton method converges to unphysical solutions.

$$\begin{aligned} SX &= [1e-3; 1e-3; 1e-3; 1e-6; 1e-6; 1e-6; 1e-6; 1e-6; 1e-6]; \\ SY &= [1; 1; 1; 1e3; 1e3; 1e3; 1e3; 1e3; 1e3]. \end{aligned} \tag{7}$$

Downloaded From: http://proceedings.spiedigitallibrary.org/ on 07/12/2017 Terms of Use: http://spiedigitallibrary.org/ss/termsofuse.aspx

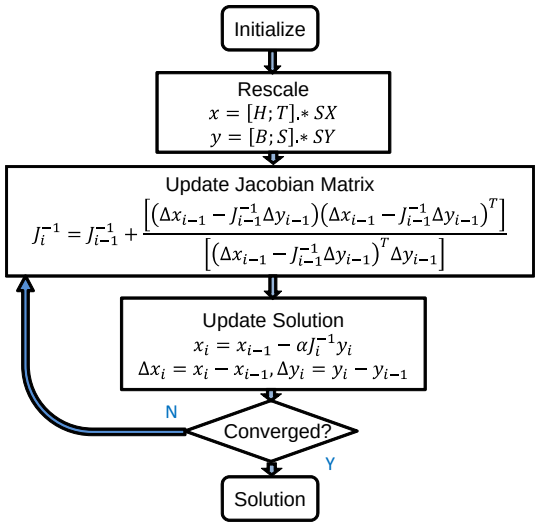

Figure 3. Flowchart of modified SR1 quasi-Newton method.

2.3 Model Modifications

(a) Modified magnetization $\mathbf{M}$ and magnetostriction $\mathbf{S}m$ equations

The bulk magnetization and magnetostriction have been expressed as weighted averages over the six crystal easy axes,[1,3,5]

$$\begin{aligned} \mathbf{M}_i &= M_s \sum_{k=1}^{6} [m_{i-1}^k (\xi_{i-1}^k + d\xi_i^k)], \\ \mathbf{S}m_i &= \sum_{k=1}^{6} [S_{i-1}^k (\xi_{i-1}^k + d\xi_i^k)]. \end{aligned} \tag{8}$$

All the components except $d\xi_i^k$ depend on previous step results. However, the magnetization $M_s m^k$ and magnetostriction S^k along the k^{th} moment orientation should be evaluated at current $\mathbf{H}$ and $\mathbf{T}$, in other words, the new equations should be written as:

$$\begin{aligned} \mathbf{M}_i &= M_s \sum_{k=1}^{6} [m_i^k (\xi_{i-1}^k + d\xi_i^k)], \\ \mathbf{S}m_i &= \sum_{k=1}^{6} [S_i^k (\xi_{i-1}^k + d\xi_i^k)]. \end{aligned} \tag{9}$$

Eq.(8) requires small step size where the current $M_s m^k$ and S^k differ slightly from stored values. However, if the previous weighted sum is applied to COMSOL, the inversion process acturally returns $(d\mathbf{H}, d\mathbf{T})$. Furthermore, $\mathbf{H}_i = \mathbf{H}_{i-1} + d\mathbf{H}$ and $\mathbf{T}_i = \mathbf{T}_{i-1} + d\mathbf{T}$, so the inversion error will accumulate leading to unphysical solutions. The inverse model designed on the basis of Eq.(9) does not purely depend on field and stress increment, so errors do not accumulate during simulation.

(b) Choice of coefficient c

According to the explanation in Section 2.3(a), the key for model convergence is to reduce the weight of incremental terms $(d\xi_{irr})$ in the constitutive model. The optimized c value is usually between 0.1-0.2,[10] which means over 80% of the $d\xi$ depends on $d\xi_{irr}$ and the majority of the material model is in incremental form. Hence, a small step size is required to maintain convergence. To reduce the influence of incremental terms, either increasing c or decreasing k_p is necessary. Hysteresis width is sensitive to the value of k_p, but c has relative small influence on minor loop width when it is smaller than 0.5. A value $c = 0.4$ is selected which provides a good balance between efficiency and accuracy.

Downloaded From: http://proceedings.spiedigitallibrary.org/ on 07/12/2017 Terms of Use: http://spiedigitallibrary.org/ss/termsofuse.aspx

(c) Negative susceptibility

In previous hysteretic Galfenol models, ζ is forced to take a value of 1 when the calculated magnetic susceptibility is positive, otherwise it switches to 0. This 0 and 1 switching can cause simulation instabilities. One of the necessary conditions in the quasi-Newton method is that the function should be first order differentiable. In this study, ζ is always 1 to smooth the material model, and simulation results do not exhibit negative susceptibility.

(d) Anhysteretic and hysteretic model switch

Fig. 4 shows flux density versus stress responses for increasing bias fields. Two key characteristics are observed in the field-induced saturation region. First, dB/dT is small, which means **T** and **H** are sensitive to the variation of **B**. A small perturbation of flux density causes large variation of field and stress, and the hysteretic EA model which is partially incremental cannot provide a converging solution. The other characteristic is that the anhysteresis curves almost coincide with the hysteretic ones at saturation. That is because all the moments have been aligned along the field direction, no moment rotation occurs, and hysteresis is negligible. This phenomenon makes it possible to replace the hysteretic model with the anhysteretic one in the saturation region. In this study, when $B > 1.37$ T, anhysteretic model automatically starts.

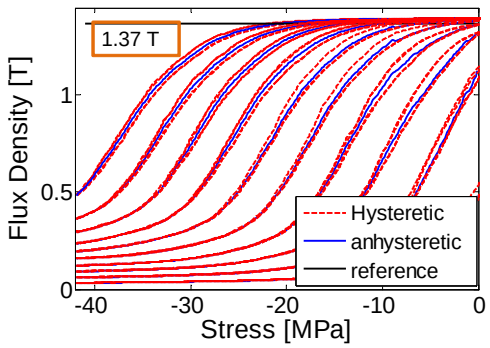

Figure 4. Comparison of hysteretic experimental results and calculated anhysteretic curves.

(e) Quasi-Newton method and Trust-Region-Reflective (TRR) method

In practice, the relationship between input (**H**,**T**) and output (**B**,**S**) is one to one reflection. In other words, only one group of (**H**,**T**) can be found for a given (**B**,**S**). However, the hysteretic EA model is accurate only when input variations are small between two continuous simulation steps. For example, if $c = 0.4$, the model should be limited to $|dH| <= 0.12$ kA/m and $|dT| <= 0.2$ MPa for a physical response. Outside of this this range, unphysical values of (H,T) can generate a seemingly physical response. The converged solution of the quasi-Newton method only relies on the initial guess. Moreover, there are no convenient and reliable ways to select initial conditions such that the converged solution is guaranteed to be physically meaningful. Another numerical method that can search solutions within a given domain should be added. Matlab has a TRR method based function(fmincon). Each instance the SR1 method returns unphysical values for (H,T), the TRR method is used.

(f) Air gap and mesh quality

Initially, the air gap between the Galfenol rod and flux return path was ignored in order to reduce the degrees of freedom. However, this simplified model cannot converge when current drives the material near to the saturation state. Fig. 5 shows the flux density distribution near the contact region between the flux return path and the Galfenol rod. Without considering the air gap, flux concentrates in a small region of the rod, and this large flux density (maximum $|\mathbf{B}| = 1.512$ T is

Downloaded From: http://proceedings.spiedigitallibrary.org/ on 07/12/2017 Terms of Use: http://spiedigitallibrary.org/ss/termsofuse.aspx

observed in Fig. 5) is unrealistic and causes lack of convergence. Furthermore, the mesh quality is also a factor that influences convergence. In this study, a "normal" mesh is used for Galfenol, a "coarse" mesh is defined for passive domains.

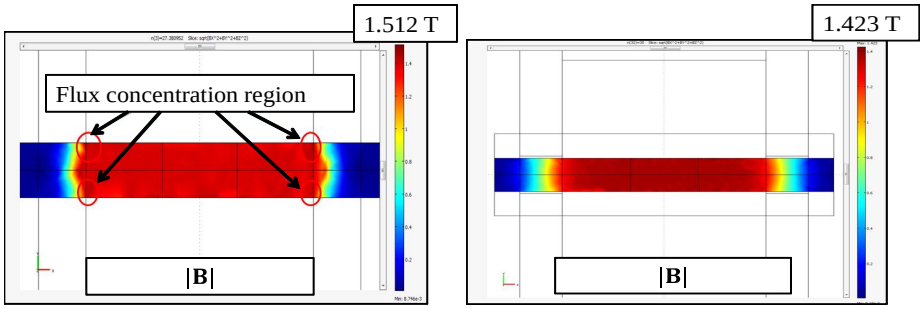

Figure 5. |**B**| on the Galfenol rod with (right) and without (left) air gap.

3. RESULTS AND DISCUSSION

3.1 Simulation Results

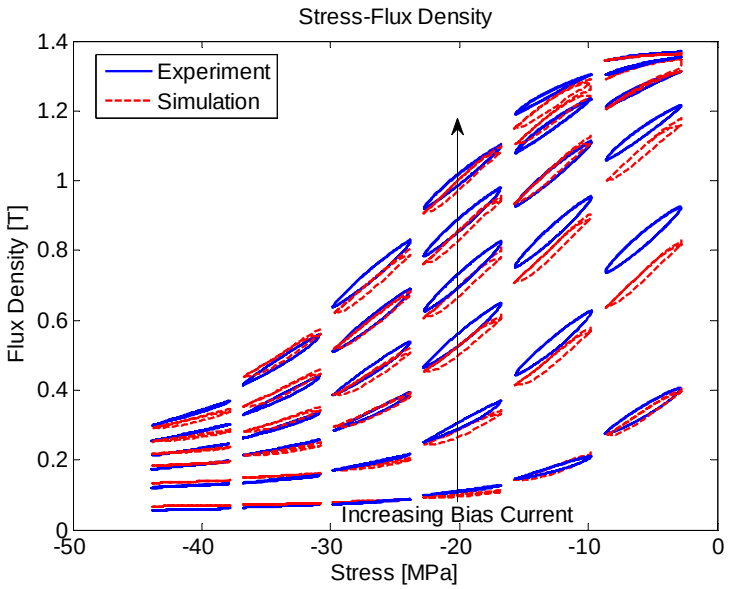

Figure 6. Stress-flux density minor loops.

Fig. 6 shows the flux density versus stress minor loops at different bias currents. Each hysteresis loop starts from a bias point which is calculated with the 3D anhysteretic model. The model results will gradually shift from anhysteretic bias points to the hysteretic minor loop in the first half cycle. After 1.5 cycles, the model converges to a complete and closed minor loop. It can be observed that the 3D hysteretic model can generally follow the trends of minor loop especially in the burst region. Fig. 7 shows field vs. stress calculations and data at different bias currents. It can be noticed that the T-H curve is more accurate when the stress is neither too small nor too large. This phenomenon will be explained in Section 3.2. The width of the hysteresis loop is correctly modeled and this validates the application of this model in the area where the energy loss is the main issue. This 3D model is initially designed to characterize stress-flux density curves and implemented to realize optimized design for Galfenol force sensors. Thus, the slope of the minor loop is the key factor that

Downloaded From: http://proceedings.spiedigitallibrary.org/ on 07/12/2017 Terms of Use: http://spiedigitallibrary.org/ss/termsofuse.aspx

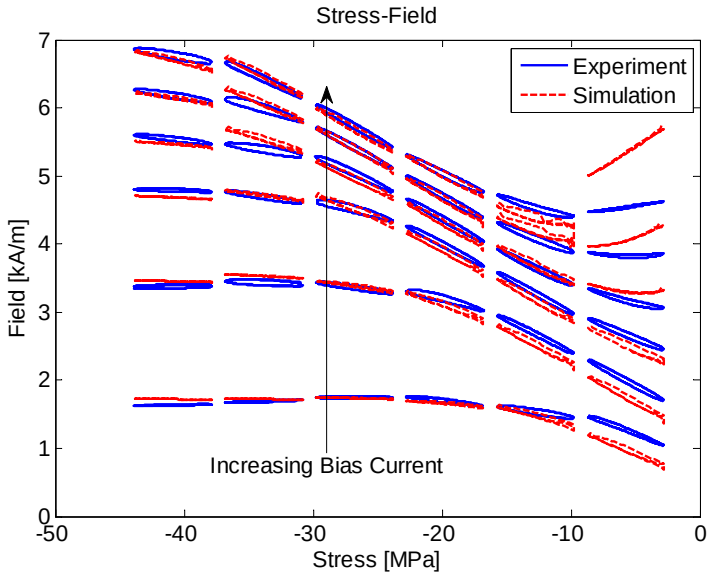

Figure 7. Stress-field minor loops.

should be used to quantify the simulation error. Linear regression is used to calculate the average slopes of all the minor loops (ignoring the initial half cycle). Both simulation and experimental results are shown in Table 1 and in Fig. 8.

Table 1. Comparison of simulation and experiment [1e-4*T/(kA/m)].

Bias Current [mA]	Center Stress [MPa]	5.8	12.8	19.8	26.8	33.8	40.8
98	Experiment	215.2	105.3	46.71	24.28	13.54	8.163
	Simulation	225.8	116.4	28.93	10.39	6.872	5.763
204	Experiment	310.6	299.0	189.7	75.40	35.24	18.41
	Simulation	320.6	276.3	153.6	48.73	18.56	11.95
288	Experiment	259.56	328.1	296.4	178.5	74.90	39.07
	Simulation	305.7	325.7	267.6	152.3	47.06	18.90
338	Experiment	172.90	301.68	322.9	248.4	120.2	57.56
	Simulation	191.1	309.1	306.8	212.4	104.0	28.98
384	Experiment	88.48	254.6	316.4	288.7	181.9	79.61
	Simulation	98.59	254.3	320.2	269.4	162.0	48.38
426	Experiment	43.91	188.0	292.1	307.3	233.7	114.7
	Simulation	30.87	228.2	311.1	296.0	214.4	79.18

3.2 Error Analysis

(a) Parameter optimization error

Chakrabarti and Dapino[10] have introduced the parameter optimization process for the anhysteretic EA model. Table 2 shows the parameters used in this study, and Fig. 9 compares the material model results with 1D measurements. The best choice for c is 0.152, but $c = 0.4$ reduces computation time and maintains reasonable accuracy. Finally, the model exhibits 3.07% and 2.2% error for sensing and actuation, respectively.

(b) Permeability error

This COMSOL FEM model also simulates the current-magnetic field (i-H) relation using Maxwell's equations. The modeling error for i-H is another error source. The permeability is related to the magnetic reluctance, which is the main factor that influences the i-H accuracy. By definition, the permeability of Galfenol, $\mu_G = \frac{dB}{dH}$, the parameter fitting error would be amplified during

Downloaded From: http://proceedings.spiedigitallibrary.org/ on 07/12/2017 Terms of Use: http://spiedigitallibrary.org/ss/termsofuse.aspx

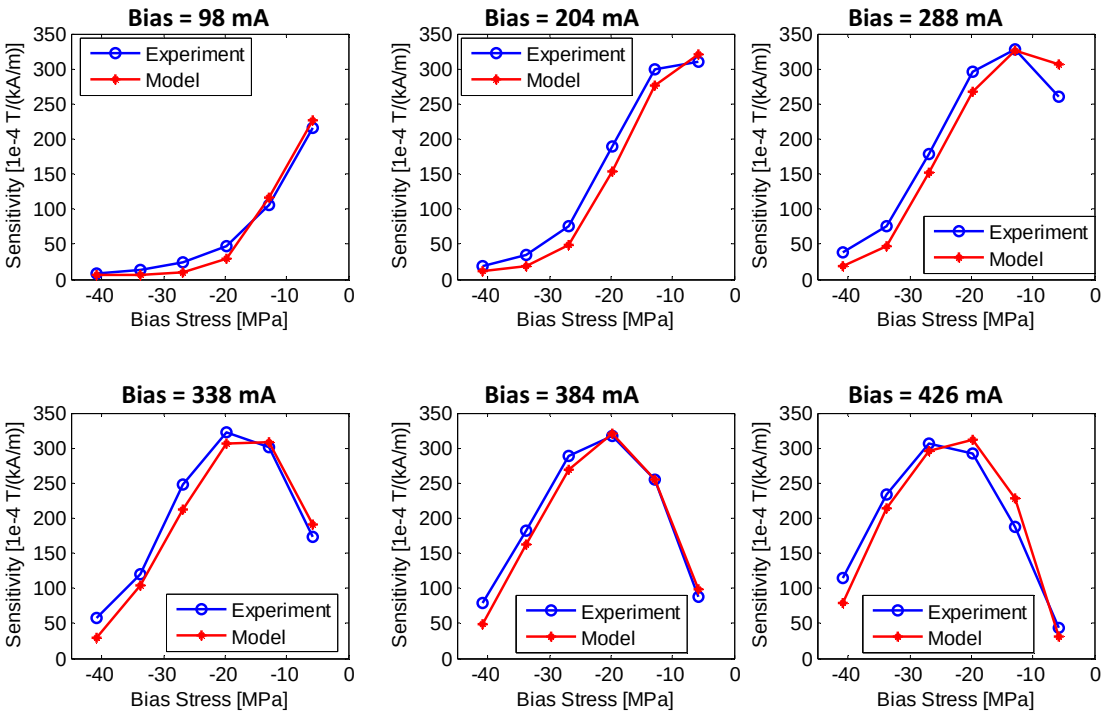

Figure 8. Sensitivity under diffenent bias currents.

Table 2. Optimzied Material Parameters

K	K_0	$\mu_0 M_s$	λ_{100}	λ_{111}
28.685e3	-0.118e3	1.3662	159.81e-6	0
E	G	a	k_p	c
58e9	120e9	774.75	400	0.4

this differentiation. Fig. 10 shows the discrepancy of permeability results between simulation and experiment. This amplified error in permeability explains the large discrepancies observed in Fig. 7 at low applied stress.

(c) Hysteresis width error

The optimized c value ought to be 0.152, but a small c requires extremely small simulation step size. Fig. 11 shows how the hysteresis model varies with c. Parameter c does not change the width of the hysteresis loop when it is smaller than 0.5, but it will flatten the slope near the saturation region as c increases. A choice of $c = 0.4$ would bring a larger relative error than the optimized $c = 0.152$.

4. SUMMARY

This paper starts from a 3D anhysteretic FEM model. Several modifications are implemented to improve the convergence of the Chakrabarti and Dapino model in large stress and field inputs simulations. The energy averaged hysteresis model is extended to 3D FEM cases. Simplification and approximation methods are introduced to overcome the weakness of the incremental hysteresis model and simultaneously achieve computational efficiency. The model is validated using a $<$ 100 $>$ oriented textured polycrystalline $Fe_{18.4}Ga_{81.6}$ rod in quasi-static condition. Comparison of simulations and experiments proves that the 3D hysteretic model is accurate over various bias current and input stress ranges. Based on this quasi-static hysteretic FEM modeling, a dynamic model for minor loop response will be built. Frequency-dependent stress-flux density minor loops measured by Walker et al.[11] are available to validate the future 3D hysteretic dynamic FEA model.

Downloaded From: http://proceedings.spiedigitallibrary.org/ on 07/12/2017 Terms of Use: http://spiedigitallibrary.org/ss/termsofuse.aspx

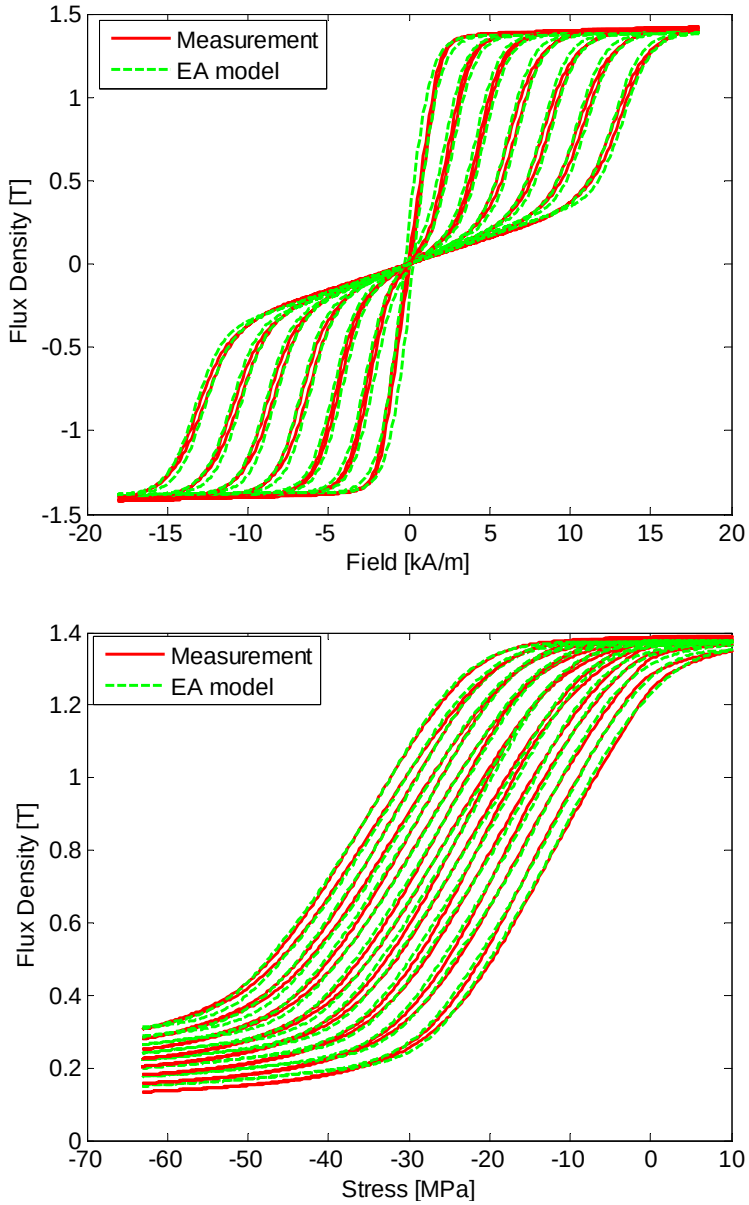

Figure 9. Parameter optimization results. Upper: Flux density vs. field at different bias stresses; Lower: Flux density vs. stress at different bias field.

Downloaded From: http://proceedings.spiedigitallibrary.org/ on 07/12/2017 Terms of Use: http://spiedigitallibrary.org/ss/termsofuse.aspx

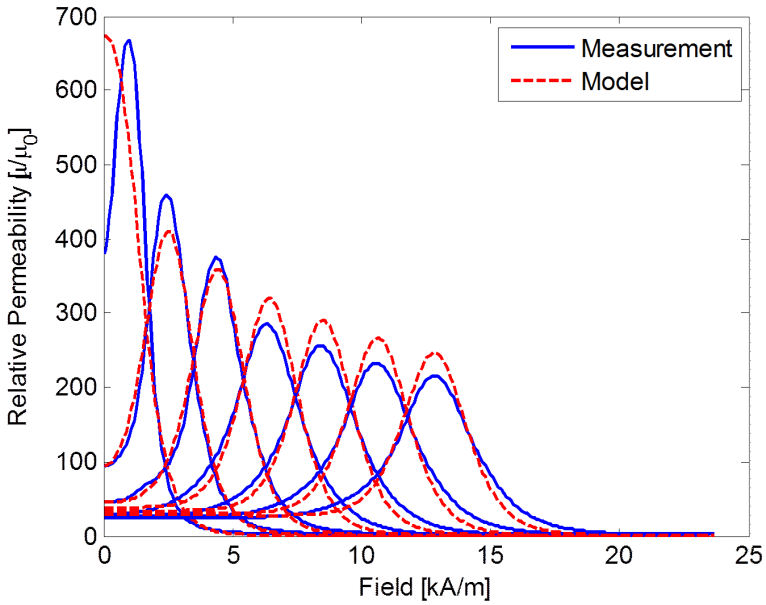

Figure 10. Parameter optimization results of permeability.

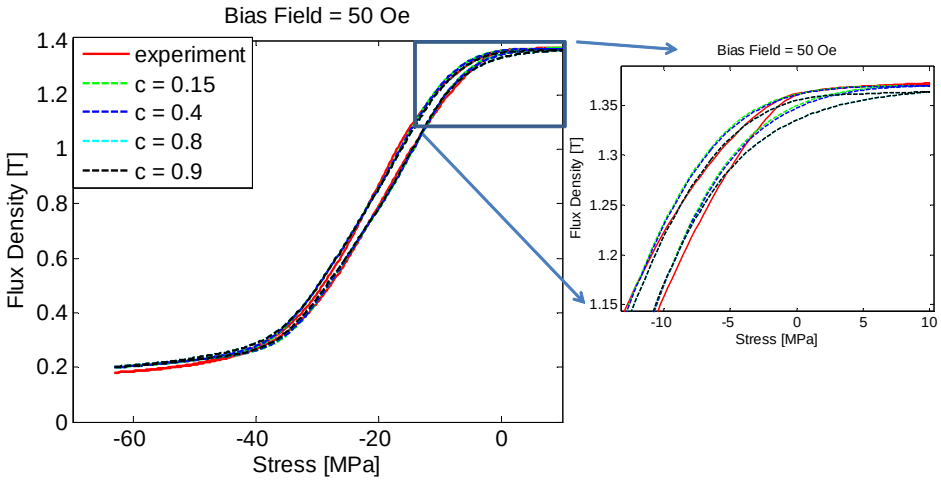

Figure 11. Hysteresis width with respect to different c values.

Downloaded From: http://proceedings.spiedigitallibrary.org/ on 07/12/2017 Terms of Use: http://spiedigitallibrary.org/ss/termsofuse.aspx

Currently, this FEA framework requires that the easy direction of Galfenol aligns along the input stress and field direction. A coordinate transformation strategy can be added to extend this model to arbitrary input directions.

ACKNOWLEDGMENTS

We wish to acknowledge the member organizations of the Smart Vehicle Concepts Center, a National Science Foundation Industry/University Cooperative Research Center (www.SmartVehicleCenter.org). We also acknowledge L. Weng and T. Walker for experimental data used in this study.

REFERENCES

1. P. G. Evans, M. J. Dapino, "Efficient magnetic hysteresis model for field and stress application in magnetostrictive Galfenol," *J. Appl. Phys.*, Vol. 107, no. 6 (2010).
2. P. G. Evans, "Nonlinear Magnetomechanical Modeling and Characterization of Galfenol and System-Level Modeling of Galfenol-Based Transducers," *PhD dissertation*, The Ohio State University, (2009).
3. L. Shu, M. J. Dapino, P. G. Evans, D. Chen, Q. Lu, "Optimization and Dynamic Modeling of Galfenol Unimorphs," *Journal of Intelligent Material Systems and Structures* 22, no. 8, 781-793 (2011).
4. S. Chakrabarti, M. J. Dapino, "A dynamic model for a displacement amplified magnetostrictive driver for active mounts," *Smart Material and Structures* 19, no. 5, (2010): 055009.
5. S. Chakrabarti, M. J. Dapino, "Nonlinear finite element model for 3D Galfenol systems," *Smart Material and Structures* 20, no. 10, (2011): 105034.
6. L. Weng, T. Walker, Z. Deng, M. J. Dapino, B. Wang, "Major and minor stress-magnetization loops in textured polycrystalline $Fe_{18.4}Ga_{81.6}$ Galfenol," *J. Appl. Phys.* Vol. 113, no. 2, (2013).
7. P. Evans, M. J. Dapino, "Dynamic Model for 3-D Magnetostrictive Transducers," *Magnetics, IEEE Transactions*, Vol.47, no. 1, (2011).
8. W. D. Armstrong, "Magnetization and magnetostriction processes in Tb(0.27-0.30)Dy(0.73-0.70)F3(1.9-2.0)," *J. Appl. Phys.*, 81, 2321 (1997);
9. P. Evans, M. J. Dapino, "Efficient model for field-induced magnetization and magnetostriction of Galfenol," *J. Appl. Phys.*, Vol. 105, no. 11 (2009).
10. S. Chakrabarti, M. J. Dapino, "Parameter Estimation of a Discrete Energy-Averaged Model from 1D Measurements", *Journal of Intelligent Material Systems and Structures*, under review.
11. T. Walker, "Sensing Behavior of Galfenol (FeGa) Alloys under Dynamic Conditions," MS Thesis, The Ohio State University, (2011).

Downloaded From: http://proceedings.spiedigitallibrary.org/ on 07/12/2017 Terms of Use: http://spiedigitallibrary.org/ss/termsofuse.aspx